Petrology of the Yugu peridotites in the Gyeonggi Massif, South Korea: Implications for its origin and hydration process

Island Arc (2008) **17,** 485–501

Thematic Article

Petrology of the Yugu peridotites in the Gyeonggi Massif, South Korea: Implications for its origin and hydration process

Shoji Arai,[1]* Akihiro Tamura,[1] Satoko Ishimaru,[1] Kazuyuki Kadoshima,[1] Yong-Il Lee[2] and Ken-ichiro Hisada[3]

[1]*Department of Earth Sciences, Kanazawa University, Kanazawa 920-1192, Japan (email: ultrasa@kenroku.kanazawa-u.ac.jp),* [2]*School of Earth and Environmental Sciences, Seoul National University, Seoul 151-747, Korea, and* [3]*Graduate School of Life and Environmental Sciences, University of Tsukuba, Tsukuba 305-8572, Japan*

Abstract Peridotites exposed in the Yugu area in the Gyeonggi Massif, South Korea, near the boundary with the Okcheon Belt, exhibit mylonitic to strongly porphyroclastic textures, and are mostly spinel lherzolites. Subordinate dunites, harzburgites, and websterites are associated with the lherzolites. Amphiboles, often zoned from hornblende in the core to tremolite in the rim, are found only as neoblasts. Porphyroclasts have recorded equilibrium temperatures of about 1000°C, whereas neoblasts denote lower temperatures, about 800°C. Olivines are $Fo_{90–91}$ in lherzolites and Fo_{91} in a dunite and a harzburgite. The Cr# (= Cr/(Cr + Al) atomic ratio) of spinels varies together with the Fo of olivines, being from 0.1 to 0.3 in lherzolites and around 0.5 in the dunite and harzburgite. The Na_2O content of clinopyroxene porphyroclasts is relatively low, around 0.3 to 0.5 wt% in the most fertile lherzolite. The Yugu peridotites are similar in porphyroclast mineral chemistry not to continental spinel peridotites but to sub-arc or abyssal peridotites. Textural and mineralogical characteristics indicate the successive cooling with hydration from the upper mantle to crustal conditions for the Yugu peridotites. Almost all clinopyroxenes and amphiboles show the same U-shaped rare earth element (REE) patterns although the level is up to ten times higher for the latter. The hydration was associated with enrichment in light REE, resulting from either a slab-derived fluid or a fluid circulating in the crust. The mantle-wedge or abyssal peridotites were emplaced into the continental crust as the Yugu peridotite body during collision of continents to form a high-pressure metamorphic belt in the Gyeonggi Massif. The peridotites from the Gyeonggi Massif exhibit lower-pressure equilibration than peridotites, with or without garnets, from the Dabie–Sulu Collision Belt, China, which is possibly a westward extension of the Gyeonggi Massif.

Key words: alpine-type peridotites, continental crust, Korean peninsula, metasomatism, spinel lherzolites, Yugu.

INTRODUCTION

Mantle-derived peridotites are occasionally exposed along plate boundaries; they have been recovered from mid-ocean ridges (divergent plate boundaries) (Aumento & Loubat 1971; Dick 1989) and oceanic fracture zones (translational plate boundaries) (Bonatti 1976; Dick 1989). Peridotite or serpentinite bodies sometimes form part of suture zones tracing former convergent plate boundaries (Coleman 1977). Despite their tectonic importance, only limited information on the petrological nature of peridotite bodies has been available on the Korean peninsula, where felsic igneous and metamorphic rocks are predominant, and peridotitic and related rocks are only sparsely and narrowly distributed (Lee 1987; Wee *et al.* 1994).

*Correspondence.

Received 3 May 2007; accepted for publication 9 January 2008.

doi:10.1111/j.1440-1738.2008.00633.x

These have been described and discussed mainly in the context of alteration and related mineralization (Chi & Kim 1977; Hwang *et al.* 1988, 1993; Woo *et al.* 1991; Kim *et al.* 1993) except for several descriptions (Wee *et al.* 1994; Song *et al.* 1997; Song & Song 2001; Seo *et al.* 2005).

The southwestern part (Cheongyang and Hongseong areas) of the Gyeonggi Massif is characterized by distribution of small peridotite bodies (Oh *et al.* 2004). The peridotites in the Gyeonggi Massif have been interpreted to be of alpine-type, namely a slice of mantle peridotite, in which dunites and harzburgites are predominant (Song *et al.* 1997; Song & Song 2001). Seo *et al.* (2005) examined the Bibong and Baekdong peridotite bodies in the Gyeonggi Massif, and unraveled varieties of petrographical and petrological characteristics caused by their different metamorphic and metasomatic histories. Some of the peridotites are fresh, and this part of the Gyeonggi Massif is an ideal locus to clarify the process of mantle peridotite intrusion into continental crust. In this paper, we report petrological and mineral chemical characteristics of the Yugu peridotite body distributed about 18 km to the northeast of the Bibong and Baekdong peridotite bodies to reveal the mantle and crustal processes of the peridotites tectonically emplaced within the continental crust. As far as we know, the Yugu peridotite body is the largest and freshest in the Gyeonggi Massif, and thus, offers advantages for analyzing mantle and uplift processes recorded in the peridotite body. Trace element mineral chemistry of pyroxenes and amphiboles especially highlight geochemical signatures on cooling and hydration of the mantle peridotites *en route* to the crustal level. Moreover, our data constrain petrological and geochemical characteristics of the peridotites in the Gyeonggi Massif.

GEOLOGICAL BACKGROUND

The study area belongs to the southwestern part of the Gyeonggi Massif, which is mainly composed of Precambrian metamorphic rocks (Kim *et al.* 1999) (Fig. 1). Its southeastern part is bounded by the northeast-trending Gongju (or Gongju–Eumseong) Fault, which forms the northwestern boundary of the Okcheon Belt, and its strike–slip motion was activated during the Early Cretaceous (Okada & Sakai 1993; Lee 1999). The sense of its movement was sinistral, resulting in the formation of the Lower Cretaceous sedimentary basin, the Gongju Basin. Strike–slip fault tectonics have played an important role in the formation of the tectonic framework in the Asian continental margin, from Sikhote–Alin to South China through the Korean peninsula since the Jurassic (Xu *et al.*

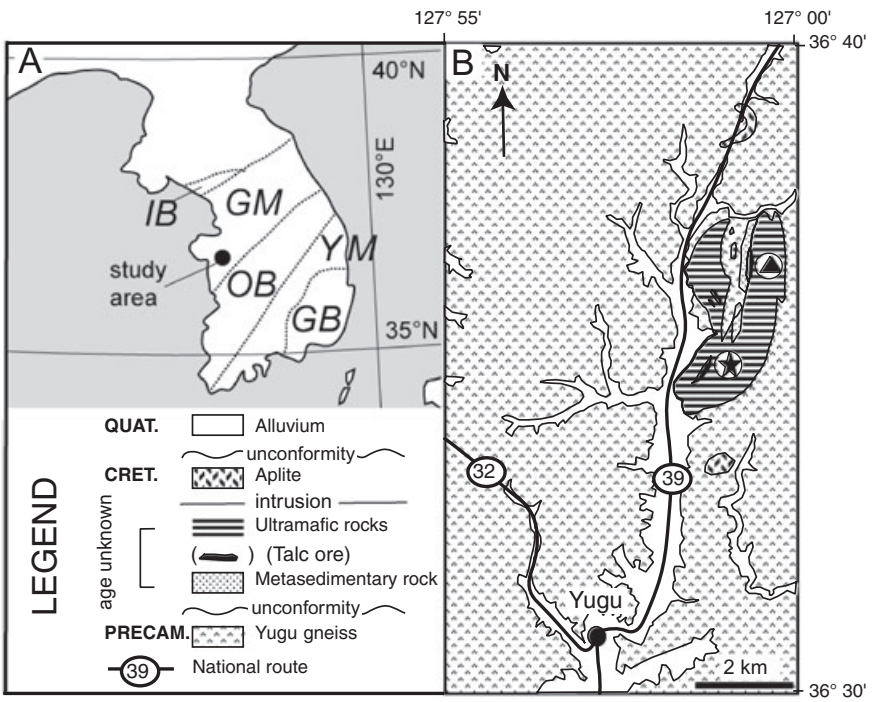

Fig. 1 Geological sketch of the Yugu peridotite body. (a) tectonic division of the Korean peninsula with the location of the study area (Yugu area) of the Korean Peninsula. IB, Imjingang Belt. GM, Gyeonggi Massif. OB, Okcheon Belt. YM, Yeongnam Massif. GB, Gyeonsang Basin, (b) geological map of the Yugu area (modified after Um & Lee 1963; Woo *et al.* 1991). Mount Geumgye (▲), the studied section (★).

1989). Several isolated ultramafic bodies are distributed in the southwestern part of the Gyeonggi Massif (Cheongyang and Hongseong areas), close to the Gongju Fault (Wee *et al.* 1994; Oh *et al.* 2005; Seo *et al.* 2005; Kim *et al.* 2006). Their trend is parallel to the NNE-trending faults, dominantly developed in that part of the Gyeonggi Massif (Woo *et al.* 1991; Wee *et al.* 1994; Yun *et al.* 1994). The Baekdong body is, however, elongated WNW–ESE, being discordant to other bodies (Seo *et al.* 2005). The peridotite body in the Yugu area is the largest and has a horseshoe shape (Fig. 1).

The study area mostly comprises the Precambrian Yugu gneiss and minor age-unknown metasedimentary rocks and ultramafic rocks (Fig. 1B). The Yugu gneiss was first named as the Yugu granitic gneiss of Jurassic age (Um & Lee 1963), but was renamed as the Precambrian Yugu gneiss by the Geological and Mineralogical Institute of Korea (1973) and Kang and Lim (1974). The Yugu gneiss was dated to be 2150 ± 20 Ma (Lee *et al.* 1973) or, more recently, *ca* 1863 Ma by sensitive high mass-resolution ion microprobe (SHRIMP) zircon age (Kim *et al.* 2006). It is composed of banded and augen structured biotite gneisses, which show gradational variation between them. It comprises quartz, plagioclase, alkali feldspar, biotite, amphibole, garnet, and chlorite with minor sillimanite, apatite, and magnetite. The Yugu gneiss is interpreted to have experienced regional metamorphism of greenschist to amphibolite facies (Chi & Kim 1977; Lee & Choi 1994). Regionally, it shows well-developed foliation with dominant N60°E strike and 70–80°northwest dip (Woo *et al.* 1991). The foliation changes in strike and dip widely around the peridotite body. The Yugu gneiss is overlain uncomformably by the age-unknown metasedimentary rocks near Mount Geumgye in the northeastern part of the study area (Fig. 1B). The metasedimentary rocks are arenaceous in nature with easily identifiable stratification, and contain some gneiss clasts. Foliation in the metasedimentary rocks strikes mostly in the east–west direction and dips to the northwest (Woo *et al.* 1991). They are in sharp contact with peridotites. Similar and symmetrical orientation of foliations in both the metasedimentary rocks and peridotites suggests that they have experienced folding together after emplacement of the peridotite body (Woo *et al.* 1991). South of the peridotite body the Yugu gneiss was intruded by a small stock of Cretaceous aplite, which is composed of quartz, potassium feldspar, and biotite with minor muscovite. On both the west and east sides of the peridotite body there exist two parallel faults trending N5–10°E (Woo *et al.* 1991).

The Yugu peridotite body is located at about 36°37′N, 126°59′E (Fig. 1). Several narrow talc-alteration zones are developed in the peridotite body. In the peridotites near Mount Geumgye, 1 to 5 cm thick mafic metamorphic layers and axial plane cleavages are observed (Woo *et al.* 1991). The marginal part of the peridotite body is strongly altered as it is rich in antigorite and/or talc. The core part, about 250 m across, is relatively fresh, preserving primary textures and some primary minerals in peridotites. We mainly worked on this fresh part (Fig. 1B). Peridotites show fine stratification or foliation due to relative abundance of olivine and pyroxenes on outcrops, possibly due to deformation (Fig. 2). Pyroxene-rich layers stand out in relief on the outcrop relative to the olivine-rich part that has been selectively weathered and has a smooth surface, forming altogether the lherzolite lithology (Fig. 2). The foliation plane strikes N30 to 70°E and dips 10 to 40°N. Dunitic layers with smooth and hollow surface are rarely observed. Websterites and possible harzburgites (highly serpentinized) have been found as boulders in and around the Yugu peridotite body.

Metabasites associated with the Baekdong and Bibong peridotites record high-pressure metamorphism of up to eclogite facies (Oh *et al.* 2004, 2005; Kim *et al.* 2006). This part of the Gyeonggi Massif is considered to be the eastward extension of the Dabie–Sulu Collision Belt, where ultrahigh-pressure metamorphic rocks and associated

Fig. 2 Photograph of a typical outcrop of the Yugu peridotites with prominent banding of pyroxene-rich layers (prominent) and olivine-rich layers (hollow). The width of the white board is 30 cm.

garnet-bearing peridotites were found (Oh 2006; Oh & Kusky 2007).

PETROGRAPHY

Peridotites are strongly deformed, and mylonitic to strongly porphyritic textures are commonly observed (Fig. 3). Rounded to flattened orthopyroxenes are the most common porphyroclasts, up to 1 cm across (Fig. 3a). Olivines, chromian spinels, and, more rarely, clinopyroxenes are also found as porphyroclasts (Fig. 3b–d). The orthopyroxene porphyroclasts have exsolution lamellae only in the core (Fig. 3e,f) and are often kinked. The olivine porphyroclasts exhibit undulatory extinction and kinking. Chromian spinels, yellowish brown to brown in thin-section, are sometimes stretched to be long polygrain streaks (Fig. 3b). Clinopyroxene porphyroclasts are rather small in number and size, less than 2 mm across, and have a turbid appearance due to abundant minute inclusions and/or exsolutions (Fig. 3c,d). They have vermicular to platy inclusions (or lamellae) of

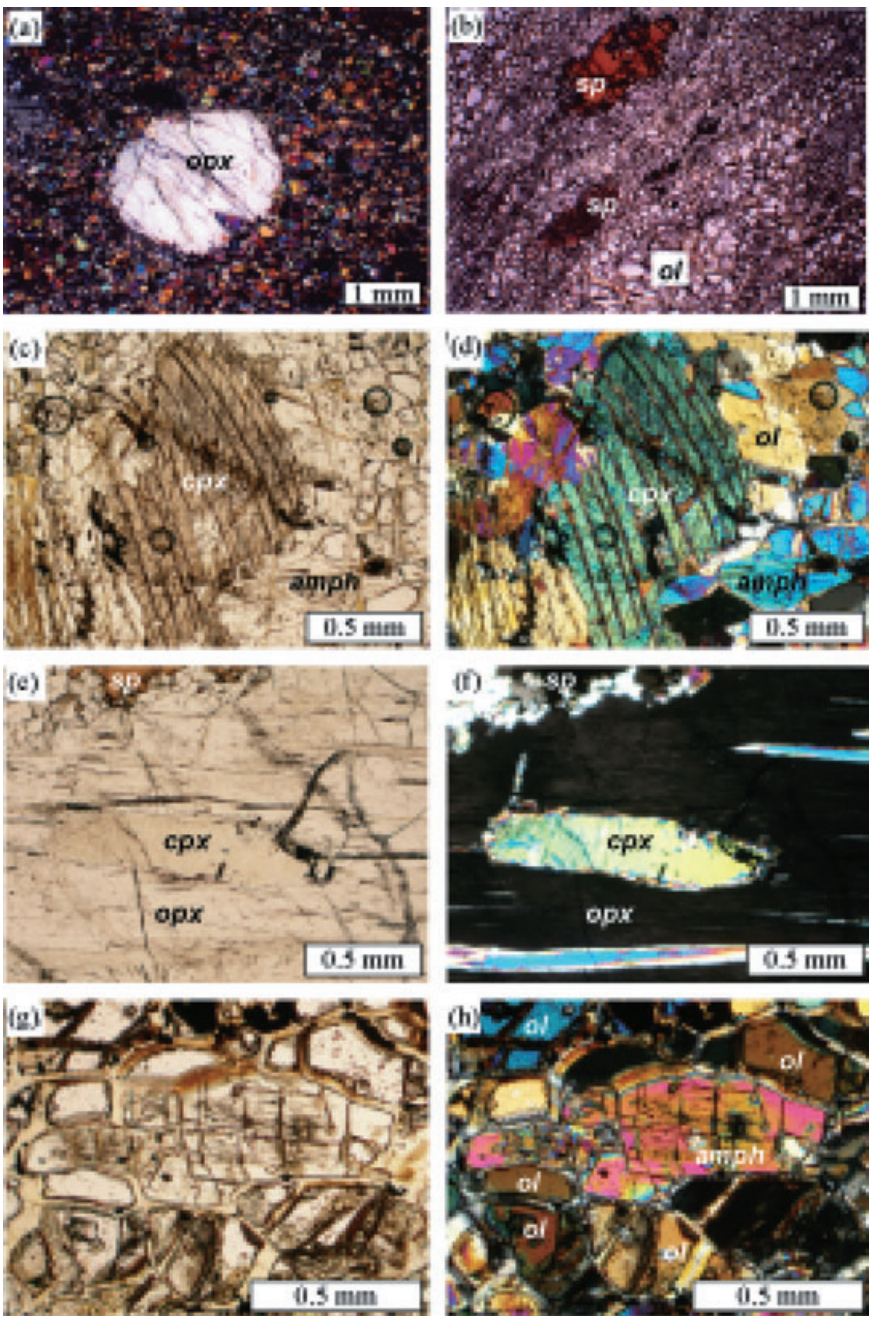

Fig. 3 Photomicrographs of the Yugu peridotites, opx, orthopyroxene; sp, chromian spinel; cpx, clinopyroxene; Amph, hornblende; ol, olivine. (a) rounded orthopyroxene porphyroclast in a mylonitized lherzolite (No. K10), crossed-polarized light, (b) porphyroclasts of chromian spinel and olivine in the mylonitized lherzolite (No. K10), plane-polarized light, (c) clinopyroxene porphyroclasts in a strongly porphyroclastic lherzolite (No. UK), note turbid appearance. Hornblende neoblasts are closely associated with the clinopyroxene porphyroclasts, plane-polarized light, (d) crossed-polarized light image of (c), (e) orthopyroxene porphyroclast with clinopyroxene lamellae and inclusion in a mylonitized lherzolite (No. K18), note clinopyroxene inclusion is clear and free of minute inclusions (cf. (c)), (f) crossed-polarized light image of (e), note that the orthopyroxene porphyroclast is free from lamellae in the rim, (g) hornblende neoblast in the strongly porphyroclastic lherzolite (No. UK), (h) crossed-polarized light image of (g), note the optical zonation of the hornblende neoblast.

colorless Al-rich spinels, which have been exsolved under subsolidus conditions. This indicates an initially Al-rich character of the clinopyroxenes. Clinopyroxene neoblasts, less commonly found than amphiboles, are clear in thin-section. Some clinopyroxene grains completely enclosed by orthopyroxene porphyroclasts are relatively clear and free of exsolution (Fig. 3e,f). Colorless amphiboles are common (sometimes abundant) as a neoblast phase of the peridotites (Fig. 3g,h). They are particularly marked around clinopyroxene porphyroclasts (Fig. 3c,d) and in the pressure shadow of orthopyroxene porphyroclasts. They show a reciprocal relationship in volume with clinopyroxenes, being smaller in amount in the peridotites that have larger amount of clinopyroxenes. Amphibole grains sometimes exhibit a zonal structure under the microscope, the rim being more birefringent than the core (Fig. 3g,h). Plagioclases are totally absent even around chromian spinels or within clinopyroxenes. The peridotites are mostly lherzolites because of abundance of clinopyroxenes and amphiboles, which were converted from clinopyroxenes, although some rocks are difficult to identify due to fine grain size of minerals.

Harzburgites show an equigranular texture with relatively fine strain-free grains, indicating textural equilibrium. Clinopyroxenes are absent, and optically zoned amphibole grains are common instead. Orthopyroxenes occur as stout prisms and are free of exsolution lamellae. Chromian spinels are rounded in shape and brown in thin-section.

Dunites suffer from much stronger serpentinization than the pyroxene-bearing peridotites. Olivines are partly preserved and the initial grain size before serpentinization was possibly up to 2 mm across, judging from optical continuity of relic olivines. Chromian spinels, less than 3% in volume, are brown in thin-section and darker in color than lherzolites. In one dunite sample especially rich in chromian spinels (>5 vol.%), both olivines and chromian spinels are completely altered, although it is found near the center of the body.

Websterites have a porphyroclastic texture, and are composed of orthopyroxenes, clinopyroxenes, and chromian spinels. Colorless amphiboles are abundant, up to 11% in volume, especially around chromian spinel and clinopyroxene grains. Orthopyroxene and clinopyroxene porphyroclasts characteristically have thick exsolution lamellae of clinopyroxene and orthopyroxene, respectively.

All of the ultramafic rocks are serpentinized to various extents (Fig. 3), but the serpentine is mainly lizardite/chrysotile formed under low-temperature conditions (Evans 1977) in the upper crustal level. Mg-chlorite and antigorite, the higher-temperature serpentine, are not found in the samples we obtained from the core of the body.

MAJOR-ELEMENT MINERAL CHEMISTRY

Minerals were analyzed by wavelength dispersive electron probe X-ray microanalysis (EPMA) (JEOL JXA8800) at the Center for Co-operative Research of Kanazawa University. Analytical conditions were 15-kV accelerating voltage, 12-nA probe current, and 3-μm probe diameter. For Ni analysis of olivines, 25-kV accelerating voltage and 20-nA probe current were adopted. Ferrous and ferric iron contents of chromian spinels were calculated assuming spinel stoichiometry, while all iron was assumed to be Fe^{2+} in silicates. Mg# and Cr# are $Mg/(Mg + Fe^{2+})$ and $Cr/(Cr + Al)$ atomic ratios, respectively. Only one sample each was analyzed for harzburgite and dunite. Selected microprobe analyses are listed in Table 1.

Olivine compositions vary from Fo_{90} to Fo_{91} in lherzolites and around Fo_{91} in a dunite and a harzburgite. The Cr# of spinels shows a positive correlation with the Fo content (= 100 Mg#) of olivines, from 0.1 to 0.3 in lherzolites and around 0.5 in the dunite and harzburgite (Fig. 4). In Figure 4, we used only data of chromian spinels within olivine-rich parts in order to minimize the subsolidus change in Cr# through reactions with pyroxenes and amphiboles. The TiO_2 content of spinels is appreciably higher in dunite than in lherzolites (Table 1). The Al-rich spinels exsolved from clinopyroxene porphyroclasts are too small for microprobe analysis.

Pyroxenes show clear differences in chemistry between porphyroclast cores and porphyroclast rims/neoblasts: Al_2O_3 and Cr_2O_3 contents are distinctly less in the latter than in the former (Table 1, Fig. 5). The core of large orthopyroxene porphyroclasts especially has high Al_2O_3 contents (>5 wt%) in fertile lherzolites (Fig. 5). Coarse orthopyroxene porphyroclasts have a distinct chemical zonation: the core is wide and chemically homogeneous, and the narrow rim is poorer in Al and Cr and richer in Mg and Si (Fig. 5, Table 1). The CaO content is slightly higher in porphyroclast cores than in neoblasts/porphyroclast rims for orthopyroxenes (Fig. 5, Table 1) and *vice versa* for clinopyroxenes. For clinopyroxenes, TiO_2 and Na_2O contents are higher and the Mg# is lower in

Table 1 Selected microprobe analyses of minerals in the Yugu peridotites

	lherzolite (K25)								lherzolite (UK)						
	Ol	Opx-1	Cpx-1-c	Cpx-1-r	Cpx-2	Sp-1	Amph-c	Amph-r	Ol	Opx-1-c	Opx-1-r	Cpx-1	Sp	Amph-c	Amph-r
SiO_2	41.12	56.36	51.77	53.43	55.53	0.00	47.72	56.54	40.86	55.30	56.41	53.84	0.00	48.61	52.39
TiO_2	0.00	0.03	0.05	0.06	0.05	0.01	0.27	0.04	0.00	0.03	0.05	0.09	0.00	0.23	0.11
Al_2O_3	0.00	3.36	4.29	3.15	0.70	55.47	12.74	2.84	0.00	4.60	3.24	2.67	49.57	11.82	7.88
Cr_2O_3	0.00	0.39	0.78	0.81	0.10	14.48	0.72	0.26	0.00	0.57	0.36	0.51	19.49	0.70	0.51
FeO*	9.27	6.15	2.02	1.85	1.44	10.98	2.71	1.80	9.27	6.43	6.28	1.72	12.50	2.68	2.27
MnO	0.12	0.19	0.06	0.07	0.07	0.12	0.04	0.05	0.14	0.17	0.19	0.05	0.18	0.04	0.08
MgO	49.84	34.51	17.72	18.12	18.17	19.93	18.81	22.55	50.32	33.96	34.38	18.13	17.93	19.18	20.98
NiO	0.39	0.09	0.06	0.04	0.05	0.30	0.10	0.10	0.40	0.08	0.07	0.06	0.23	0.13	0.11
CaO	0.02	0.23	23.74	24.41	25.31	0.00	12.87	13.39	0.02	0.31	0.27	24.34	0.00	12.87	12.86
Na_2O	0.01	0.02	0.07	0.06	0.08	0.03	1.53	0.30	0.00	0.00	0.01	0.17	0.00	1.44	0.94
K_2O	0.00	0.01	0.00	0.00	0.00	0.00	0.51	0.07	0.01	0.00	0.00	0.01	0.00	0.36	0.13
Total	100.77	101.34	100.56	102.00	101.50	101.32	98.02	97.94	101.02	101.45	101.26	101.59	99.90	98.06	98.26
Mg#	0.905	0.909	0.940	0.946	0.957	0.770	0.925	0.857	0.906	0.904	0.907	0.949	0.722	0.927	0.943
Cr#						0.149							0.209		
Mg/(YCr)		0.905	0.493	0.494	0.489	0.148				0.899	0.902	0.496	0.208		
Fe*/(YAl)		0.090	0.032	0.028	0.022	0.848				0.096	0.093	0.026	0.789		
Ca/(YFe)		0.005	0.475	0.478	0.489	0.004				0.006	0.005	0.478	0.002		

	lherzolite (K18)								lherzolite (K82)					lherzolite (K16)			
	Ol	Opx-1-c	Opx-1-r	Cpx-1-c	Cpx-2	Cpx-inc	Sp	Amph	Ol	Opx-1	Opx-2	Cpx-1	Sp	Ol	Cpx-2	Sp	Ol
SiO_2	40.67	55.09	55.87	53.27	55.80	52.64	0.00	46.25	41.01	53.95	56.99	52.48	0.06	40.90	53.86	0.78	41.01
TiO_2	0.00	0.04	0.03	0.08	0.07	0.15	0.01	0.32	0.00	0.06	0.02	0.26	0.00	0.00	0.05	0.00	0.00
Al_2O_3	0.01	4.57	2.84	2.65	0.58	4.32	54.37	13.59	0.01	5.80	2.47	4.44	57.27	0.00	1.56	43.06	0.01
Cr_2O_3	0.00	0.56	0.33	0.47	0.02	0.76	14.95	0.70	0.00	0.55	0.29	0.56	11.08	0.01	0.44	24.75	0.00
FeO*	9.56	6.46	6.28	1.76	1.45	1.88	11.41	2.83	9.76	6.51	6.89	2.04	11.74	9.14	1.44	15.81	9.76
MnO	0.16	0.16	0.16	0.05	0.05	0.04	0.14	0.03	0.13	0.10	0.15	0.02	0.08	0.18	0.04	0.24	0.13
MgO	50.17	33.89	34.05	17.75	18.28	17.07	19.32	18.09	48.98	32.85	34.66	17.45	19.42	50.00	17.61	17.01	48.98
NiO	0.41	0.09	0.07	0.05	0.06	0.05	0.28	0.07	nd	nd	nd	nd	nd	0.39	nd	nd	nd
CaO	0.01	0.57	0.25	24.58	25.48	23.70	0.01	12.97	0.02	0.32	0.22	22.53	0.04	0.00	24.54	0.01	0.02
Na_2O	0.00	0.00	0.00	0.09	0.08	0.24	0.01	1.67	0.03	0.03	0.03	0.36	0.03	0.00	0.06	0.00	0.03
K_2O	0.00	0.00	0.01	0.00	0.01	0.00	0.00	0.53	0.00	0.00	0.04	0.03	0.00	0.00	0.02	0.02	0.00
Total	100.99	101.43	99.89	100.75	101.88	100.85	100.50	97.05	99.94	100.17	101.76	100.17	99.72	100.62	99.62	101.68	99.94
Mg#	0.905	0.903	0.906	0.947	0.957	0.942	0.756	0.919	0.899	0.900	0.900	0.938	0.755	0.908	0.956	0.699	0.899
Cr#							0.156						0.115			0.278	
Mg/(YCr)		0.894	0.902	0.487	0.489	0.485	0.155			0.894	0.896	0.502	0.114		0.488	0.269	
Fe*/(YAl)		0.094	0.093	0.027	0.022	0.030	0.842			0.099	0.100	0.033	0.880		0.022	0.697	
Ca/(YFe)		0.011	0.005	0.485	0.049	0.484	0.003			0.006	0.004	0.465	0.006		0.489	0.034	

	harzburgite (K100)			dunite (K39)		websterite (KC8)		
	Ol	Opx	Sp	Ol	Sp	Opx	Cpx	Sp
SiO_2	41.19	58.41	0.03	41.61	0.02	54.81	51.37	0.00
TiO_2	0.00	0.03	0.01	0.01	0.25	0.02	0.07	0.00
Al_2O_3	0.00	0.96	23.03	0.00	27.79	5.13	5.65	54.58
Cr_2O_3	0.00	0.16	42.92	0.00	41.02	0.72	1.54	13.97
FeO*	7.87	5.03	23.00	9.05	18.95	7.14	2.10	12.53
MnO	0.12	0.18	0.20	0.07	0.33	0.13	0.11	0.19
MgO	50.64	35.93	10.59	50.75	12.75	32.53	15.97	17.64
NiO	nd	nd	nd	0.31	nd	nd	nd	nd
CaO	0.05	0.20	0.00	0.00	0.01	0.28	23.09	0.03
Na_2O	0.00	0.00	0.00	0.06	0.04	0.05	0.69	0.07
K_2O	0.00	0.02	0.02	0.05	0.05	0.02	0.02	0.03
Total	99.87	100.92	99.80	101.91	101.21	100.83	100.61	99.04
Mg#	0.920	0.927	0.493	0.909	0.572	0.890	0.931	0.703
Cr#			0.556		0.498			0.147
Mg/(YCr)	0.924		0.532		0.000	0.886	0.473	0.147
Fe*/(YAl)	0.073		0.426			0.109	0.035	0.853
Ca/(YFe)	0.004		0.042			0.005	0.492	0.000

FeO*, total iron as FeO; Mg, Fe*, Ca, atomic fractions of Mg, total Fe and Ca, respectively, over (Mg + total Fe + Ca) of pyroxenes. YCr, YAl, YFe, cationic fractions of Cr, Al and Fe^{3+}, respectively, over ($Cr + Al + Fe^{3+}$) in chromian spinel. Ol, olivine; Opx, orthopyroxene; Cpx, clinopyroxene; Sp, chromian spinel; Amph, amphibole; suffixes 1 and 2, porphyroclasts and neoblasts, respectively; c and r, cores and rims, respectively; inc, inclusions.

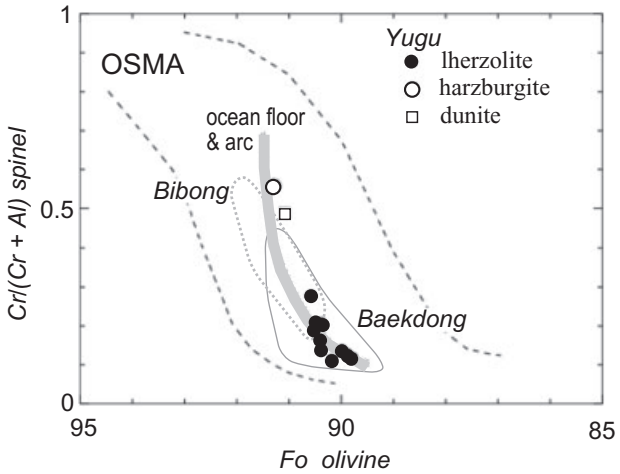

Fig. 4 Relationships between the Fo content of olivines and Cr/(Cr + Al) atomic ratio of spinels in the Yugu peridotites. Representative pairs were determined for individual samples by averaging microprobe analyses of porphyroclast phases. OMSA, olivine–spinel mantle array as a spinel peridotite residual trend (Arai 1994). Typical residual trend (thick gray line) for abyssal and Japan-arc peridotites (Arai 1994) is shown for comparison. Note that the Yugu peridotite trend is almost equivalent to that for abyssal and Japan-arc peridotites. Fields for the Bibong and Baekdong peridotites (Seo *et al.* 2005) are shown for comparison.

porphyroclast cores than in neoblasts/porphyroclast rims. The Na_2O content of clinopyroxenes is relatively low even in the porphyroclast cores, up to 0.3 to 0.5 wt% in the most fertile lherzolite that contains chromian spinels with Cr# of 0.1 (No. K82 of Table 1). Pyroxenes of websterites are similar in chemistry to those of porphyroclasts in lherzolites (Table 1).

Neoblasts of amphiboles exhibit a wide compositional range from tremolite to hornblende [magnesiohornblende to pargasite after Leake *et al.* (1997)]. They sometimes show chemical zoning from hornblende in the core to tremolite in the rim (Fig. 6). Hornblendes are characterized by relatively low contents of TiO_2 (<0.3 wt%), Na_2O (<1.8 wt%) and K_2O (<0.9 wt%) (Table 1).

TRACE-ELEMENT CHEMISTRY OF PYROXENES AND AMPHIBOLES

Trace-element concentrations of minerals (amphiboles, clinopyroxenes, orthopyroxenes) in the samples were determined by laser ablation-inductively coupled plasma mass spectrometry (193 nm ArF excimer, MicroLas GeoLas Q-plus, Agilent 7500S) (LA–ICP–MS) at Kanazawa University (Ishida *et al.* 2004; Morishita *et al.* 2005a,b). Each analysis was performed by laser-ablating spots of 50 μm in diameter at repetition rate of 5 Hz for amphibole and clinopyroxene, and 80 or 100 μm at 10 Hz for orthopyroxene, with an energy density of 8 J/cm^2 per pulse. Signal integration times of ICP–MS were 40 or 50 s for a gas background interval and 30 or 50 s for an ablation interval. NIST SRM 612 glass was used as the primary calibration standard. The element concentration of the NIST SRM 612 was selected from Pearce *et al.* (1996). Data reduction was facilitated using ^{29}Si as an internal standard for minerals, based on SiO_2 contents determined by EPMA, following a protocol identical to that outlined by Longerich *et al.* (1996). The accuracy of measurements for REE estimated from analyses of reference material (NIST SRM 614) are much better than 4% in relative standard deviation, although it depends on the abundance.

Both clinopyroxenes and amphiboles are enriched in Sr (although depleted relative to adjacent elements) and light REE, displaying U-shaped or U-shaped REE patterns with concavity at the level of middle REE (Fig. 7). Amphiboles and clinopyroxenes, except inclusions in orthopyroxene porphyroclasts, show similar trace-element patterns, although their abundances are quite different between the two minerals (Fig. 7). This possibly indicates their equilibrium regarding distribution of these elements, which are, however, substantially more partitioned to amphiboles than to clinopyroxenes (Fig. 7). Both the clinopyroxene porphyroclasts and neoblasts have the same trace-element contents, although they are distinct in major-element chemistry. Clinopyroxenes enclosed by an orthopyroxene porphyroclast in K18 show a distinctive REE pattern, monotonically decreasing from heavy REE to Nd and then increasing to La (Fig. 7). The pattern from heavy to middle REE is similar to that of residual clinopyroxenes from abyssal lherzolitic peridotites (e.g. Johnson *et al.* 1990; Kelemen *et al.* 1995) (Fig. 7). Titanium behavior is noteworthy: clinopyroxenes and amphiboles exhibit positive and negative spikes, respectively, relative to neighboring elements, although both show a negative spike for Zr (Fig. 7). Amphiboles show different levels of REE and other trace elements, especially in sample UK (Fig. 7). This is strongly dependent on the amphibole composition: the REE and trace element contents increase with an increase of Al and Na in amphiboles.

Orthopyroxenes show strongly U-shaped REE distribution patterns, of which middle REE are below detection limits (Fig. 7). It is noteworthy

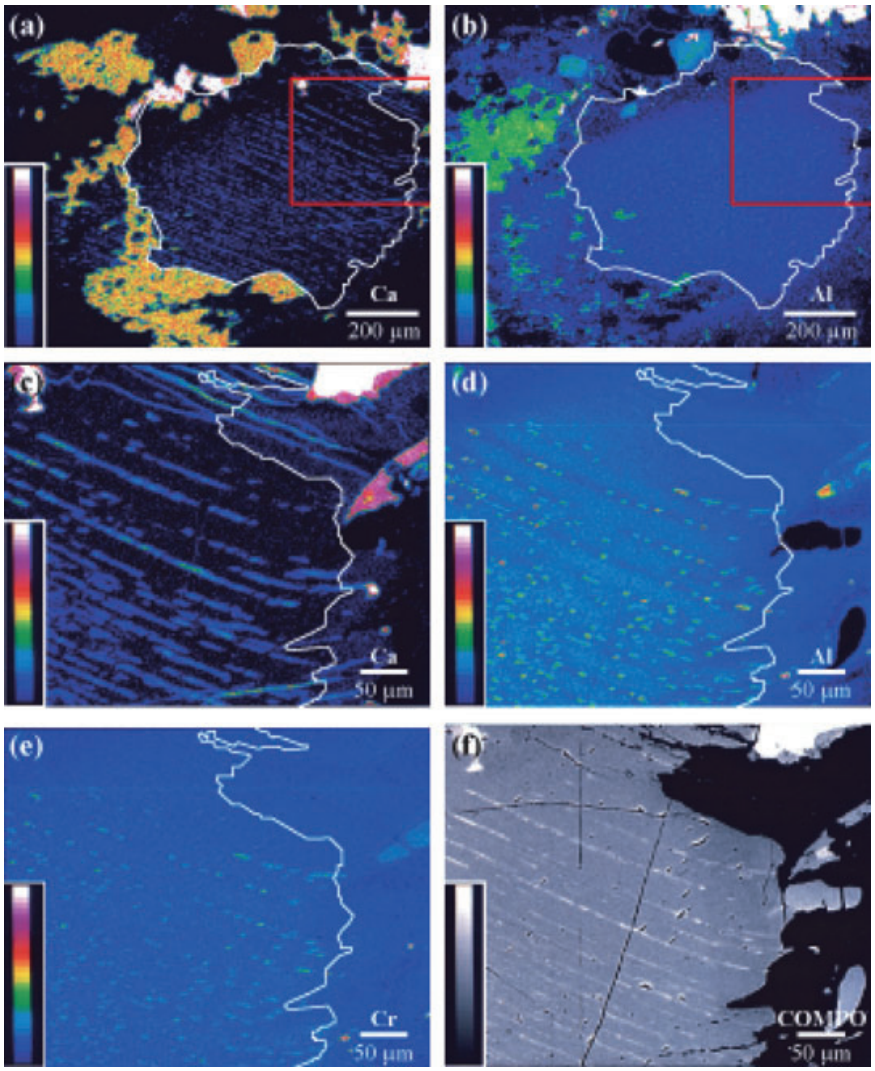

Fig. 5 Elemental distribution maps of an orthopyroxene porphyroclast in a mylonitic lherzolite (No. K18) determined with microprobe. (a) Ca, (b) Al, (c) Ca, (d) Al, (e) Cr, and (f) BSE image. The area for (c) to (f) is shown by a rectangle in (a) and (b). Note the chemical zonation of the orthopyroxene porphyroclast. Clinopyroxene lamellae are absent in the rim (a,c,f). Analysis was conducted at 20-kV accelerating voltage, 50-nA probe current, <1-μm probe diameter, and 1-μm step interval.

that they contain appreciably high amounts of light REE (Fig. 7). They display positive spikes for Ti and Zr (Fig. 7).

THERMOBAROMETRY

The equilibrium temperature for a typical porphyroclast assemblage is calculated to be 1010°C on average according to the two-pyroxene thermometer of Wells (1977). Exsolution of pyroxenes and Al-rich spinels in pyroxene porphyroclasts may indicate the presence of a higher-temperature equilibration stage. Neoblast pairs denote distinctly lower temperatures, e.g. 805°C on average (Wells 1977). Plagioclases and garnets are absent both as porphyroclasts and as neoblasts even in the most fertile lherzolite. This indicates the equilibration within the spinel lherzolite stability field both for the porphyroclast and neoblast assemblages (Fig. 8). The rim of amphibole neoblasts is sometimes tremolitic, indicating lower equilibrium temperatures obtained mainly during crustal processes (e.g. Evans 1977, 1982). Absence of chlorites and antigorite within the core of the Yugu peridotite body possibly indicates a short residence time within the stability field of these hydrous silicates.

DISCUSSION

CHARACTERIZATION OF YUGU PERIDOTITES

The peridotites had been more or less hydrated under high-temperature conditions to form amphiboles before initiation of low-temperature serpentinization (formation of chrysotile/lizardite). The amphiboles were most probably produced at

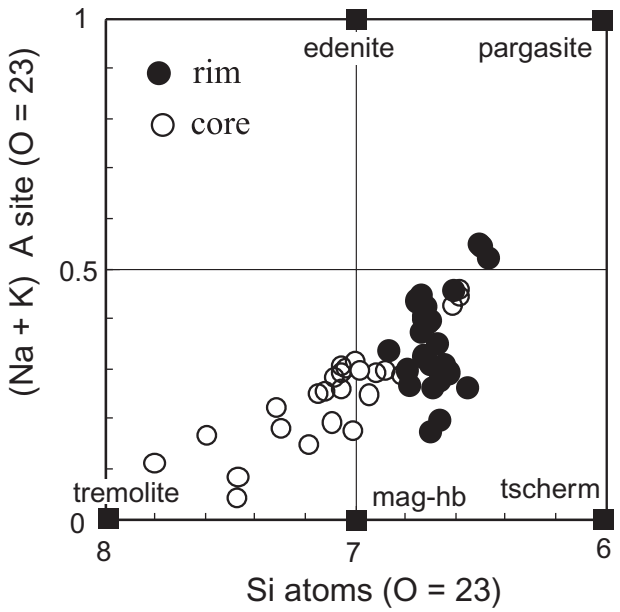

Fig. 6 Relationships between Si and (Na + K) in calcic amphibole neoblasts in the Yugu peridotites. Note that the rim tends to be tremolitic (see Fig. 3g,h). Nomenclature is for Mg-rich, Ti-poor calcic amphiboles after Leake *et al.* (1997). mag-hb, magnesiohornblende; tscherm, tschermakite.

the expense of primary clinopyroxenes, judging from their mode of occurrence, i.e. their close association with relic clinopyroxenes and the reciprocal volume relation with clinopyroxenes. Protoliths for the Yugu peridotites are spinel lherzolites, and we can examine their primary characteristics using the porphyroclast mineral chemistry described above. The olivine–spinel compositional relationship in the Yugu lherzolites indicates a residual trend attributable to a small extent of partial melting (Arai 1994) (Fig. 4). An intermediate degree of partial melting may be suggested if the harzburgite is taken into consideration (Fig. 4). The clinopyroxenes enclosed by orthopyroxene porphyroclasts in sample K18 (Fig. 3e,f) have preserved the residual magmatic character in terms of middle to heavy REE contents (Fig. 7c). Sample K18 is equivalent to slightly depleted abyssal lherzolites in terms of spinel Cr# and heavy to middle REE contents of clinopyroxenes (Hellebrand *et al.* 2001).

The Yugu peridotites are mineralogically similar to some sub-arc or abyssal peridotites (Arai 1991). They are slightly different in olivine–spinel trend from continental spinel peridotites but are apparently similar to abyssal (or ophiolitic) or sub-arc peridotites (Arai 1994) (Fig. 4). The Yugu fertile lherzolites are characterized by low Na_2O contents (0.3 to 0.5 wt%) of clinopyroxenes, and are quite different from ordinary sub-continental peridotites mainly obtained as solid intrusive peridotites and xenoliths from continental rift zones (Kornprobst *et al.* 1981; Arai 1991). Lherzolite xenoliths from Boun, Korea, representing the upper mantle material beneath the Korean peninsula, for example, contain clinopyroxenes with high (1 to 2 wt%) Na_2O contents (Arai *et al.* 2001). It is possible that the mantle residual clinopyroxenes with low Na contents were formed under relatively low-pressure conditions, namely within the upper mantle overlain by a relatively thin crust (Arai 1991; Arai *et al.* 2001). Na increasingly partitions to clinopyroxenes over associated melts with a pressure increase (Blundy *et al.* 1995). The Na content of clinopyroxene can be, however, reduced by subsolidus formation of plagioclases (Kornprobst *et al.* 1981; Bonatti *et al.* 1986) or hornblendes (Bonatti *et al.* 1986). In the Zabargad peridotites from the Red Sea, for example, the Na_2O content of clinopyroxene varies from 1 to 2 wt% in almost anhydrous spinel lherzolites to 0.5 to 0.6 wt% in plagioclase and plagioclase–amphibole peridotites (Bonatti *et al.* 1986; Bonatti 1990). The amphibole peridotites of Zabargad are, however, sometimes rich in hornblendes, up to 21 vol.%, and minerals have been much closer in equilibrium with each other: chromian spinels have become enriched in Cr and Fe after consumption of Mg–Al spinel components for hornblende formation (Bonatti *et al.* 1986). In amphibole-bearing peridotites from St. Paul's Rocks, equatorial Atlantic (Melson *et al.* 1972; Bonatti 1990), minerals do not approach equilibrium as much: amphiboles vary in chemistry from hornblende to tremolite (Roden *et al.* 1984). The Na_2O content of clinopyroxenes has been kept relatively high, around 1 wt%, in porphyroclasts, even in the amphibole-bearing peridotites of St. Paul's Rocks (Roden *et al.* 1984). In the Yugu peridotites, on the other hand, the neoblasts are distinctly in disequilibrium in major-element chemistry with the porphyroclasts, suggesting that the relatively low Na_2O content of clinopyroxene porphyroclasts has not been ascribed to subsolidus reactions but is a primary character. This may be supported by the uniformly low Na_2O content of clinopyroxene porphyroclasts independent of the degree of hydration (i.e. the amount of amphibole). This is consistent with the low bulk-rock Na_2O content (<0.1 wt%) of the Bibong peridotites, which show some petrographical similarities to the Yugu peridotites (Seo *et al.* 2005). The possible residual trend of the Fo (olivine)–Cr# (spinel) has been also

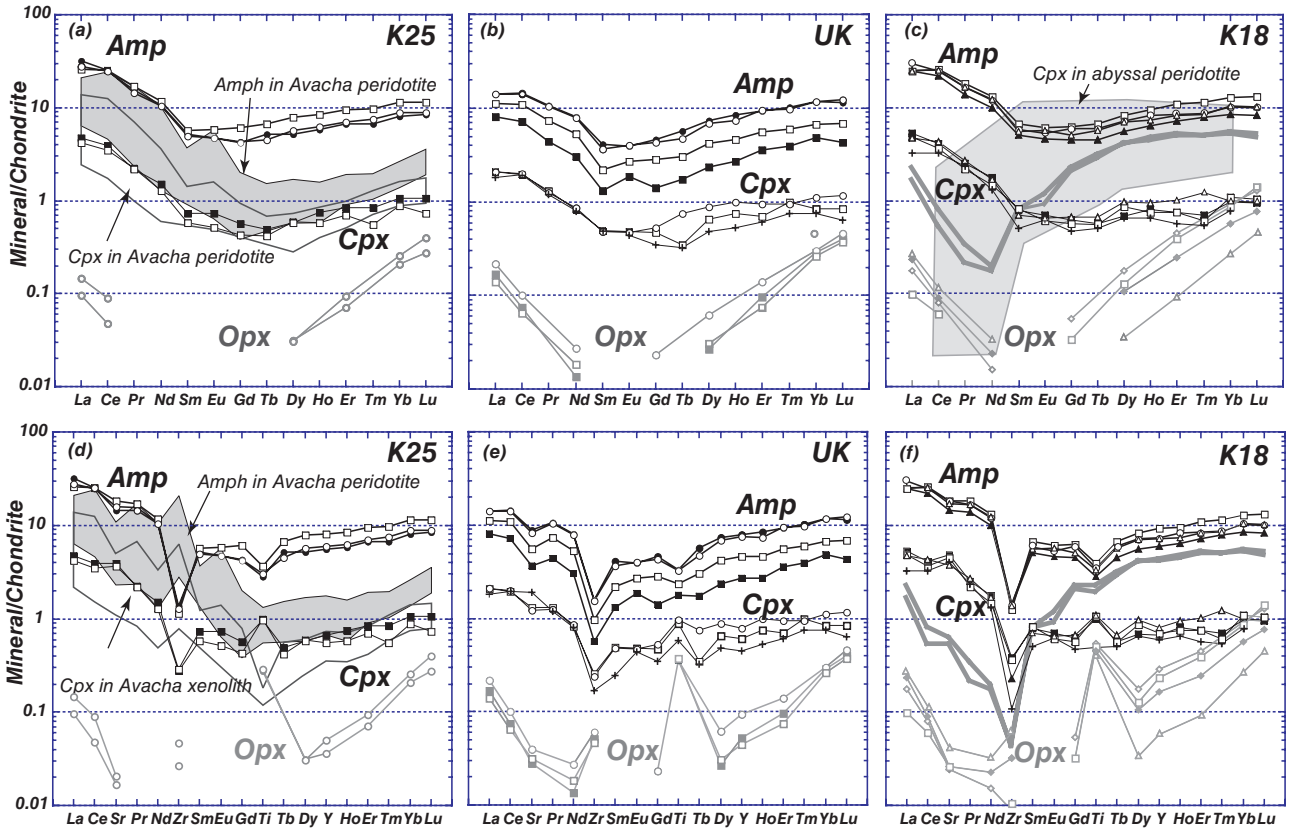

Fig. 7 (a–c) Chondrite-normalized REE and (d–f) multi-element patterns of Amph, amphiboles; Cpx, clinopyroxenes; Opx, orthopyroxenes in peridotite samples (K25, UK, K18). Chondrite values are from Sun and McDonough (1989). REE abundances are clearly different between the minerals. Note that the clinopyroxene enclosed by an orthopyroxene porphyroclast (Cpx in Opx) in K18 has relatively high-REE abundances (grey thick lines in c,f). Closed and open symbols are core and rim of each grain, respectively. Ranges of clinopyroxenes and pargasitic amphiboles in a harzburgite xenolith (#277), strongly metasomatized by slab-derived fluids, from Avacha Volcano, Kamchatka (Ishimaru *et al.* 2007) are indicated in (a,b). The range for clinopyroxenes in abyssal peridotites (Kelemen *et al.* 1995) is also shown for comparison.

barely changed during the subsolidus stage (Arai 1994). The Yugu peridotites have been probably derived from the sub-arc or abyssal upper mantle overlain by a relatively thin crust (Arai 1991).

The Yugu peridotites are similar in primary petrological character to the peridotites from Bibong and Baekdong of the same area (Seo *et al.* 2005) (Fig. 4). Dunites and harzburgites have been also reported from the Bibong and Singok areas adjacent to the Yugu area (Song *et al.* 1997; Song & Song 2001; Seo *et al.* 2005). These peridotites have been highly altered and metamorphosed to amphibolite to granulite facies, and thus, their protoliths should be carefully determined. The high Cr# character, from 0.5 to 0.6, of relic spinels probably indicates that the Singok peridotites are largely harzburgites (Song & Song 2001). This Cr# of spinel is very similar to that of the Yugu harzburgite. This kind of harzburgite is quite common in the ophiolitic mantle (Arai *et al.* 1990), indicating their derivation from the ocean floor to arc mantle (Dick & Bullen 1984; Arai 1994).

METASOMATIC MODIFICATION OF YUGU PERIDOTITE

Almost all clinopyroxenes and amphiboles are in equilibrium in terms of REEs (Fig. 7). Enrichment of light REEs and Sr relative to heavy REEs in amphiboles and pyroxenes, especially in orthopyroxenes, strongly suggests metasomatic modification of peridotites by a fluid or fluids. The involved fluid is possibly similar in chemistry to slab-derived fluids (Maury *et al.* 1992). The REE and trace-element distribution patterns of clinopyroxenes and amphiboles of the Yugu peridotites are approximately similar to those in peridotite xenoliths from the Avacha Volcano, Kamchatka Arc, which are representative of the mantle wedge material beneath a volcanic front (Fig. 7) (Ishimaru *et al.* 2007; Ishimaru & Arai 2008). The Yugu

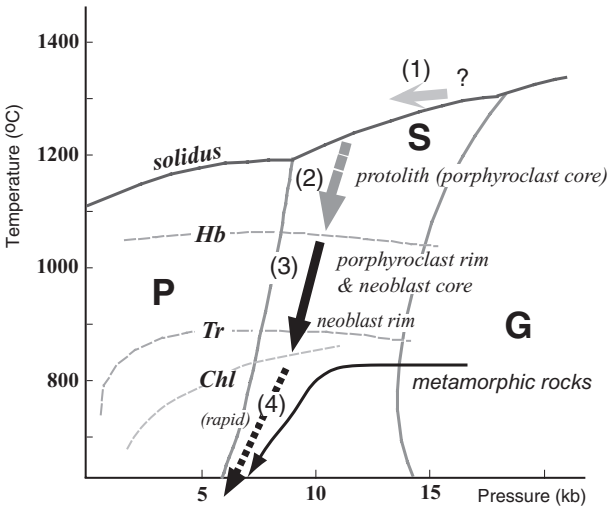

Fig. 8 Possible T–P trajectories of the Yugu peridotite: (1) formation of residual spinel peridotite as a residue after partial melting, (2) subsolidus cooling to form the protolith of the Yugu peridotite, of which relics are the present porphyroclasts, (3) cooling, shearing and hydration, during which the neoblasts were formed, and (4) relatively quick uplift of the peridotite through the plagioclase lherzolite stability field to the surface. Lherzolite phase relation is after Gasparik (1987). G, garnet lherzolite; S, spinel lherzolite; P, plagioclase lherzolite. *Hb* and *Tr*, upper stability limits of hornblende (pargasite) and tremolite, respectively, compiled by Gilbert *et al.* (1982). *Chl*, stability limit of chlorite in the peridotite system (Evans 1977). A P–T path for metamorphic rocks from Bibong (Kim *et al.* 2006) is shown for comparison.

amphiboles are also similar to metasomatic amphiboles in mantle-wedge peridotite xenoliths from Lihir, Papua New Guinea (Grégoire *et al.* 2001). The Yugu peridotites are also similar to the Finero hydrated peridotites, northern Italy (Zanetti *et al.* 1999), in trace-element characteristics of clinopyroxenes and amphiboles except for the positive spike of Ti in the Finero clinopyroxenes. The involved metasomatic fluid on the Finero peridotite was interpreted to be derived from the subducted slab (Zanetti *et al.* 1999). The metasomatism associated with hydration is due to either mantle-wedge metasomatism above a slab or crustal hydration after detaching from the mantle. Deficiency of high field strength elements (e.g. Ti and Zr) (cf. Zanetti *et al.* 1999) (Fig. 7) is not in conflict with this interpretation. The two hydration processes can be associated with cooling (cf. Okamura *et al.* 2006; Ishimaru & Arai 2008), and may be indistinguishable in terms of mineral chemistry.

The metasomatism imposed on the Yugu peridotites may be similar to that on the Bibong peridotites, which exhibit bulk-rock REE patterns (Seo *et al.* 2005) similar to the clinopyroxene and amphibole REE characteristics of the Yugu peridotites. The metasomatic agent for the Baekdong peridotites is, however, distinct from those for the Yugu and Bibong peridotites. Some of the Baekdong peridotites contain metasomatic phlogopites in addition to amphiboles, and display almost flat bulk-rock REE patterns (Seo *et al.* 2005).

It is noteworthy that partition coefficients of REEs between amphiboles and clinopyroxenes (= $^{Amph/Cpx}D$) are larger than one and approach 10 in the Yugu peridotites (Fig. 7). The $^{Amph/Cpx}D$ values are mostly 3 to 4 for the Finero peridotites (Zanetti *et al.* 1999). They are much lower, around 1 to 2, in peridotite xenoliths (Witt-Eickshen & Harte 1994; Ionov & Hofmann 1995; Vannucci *et al.* 1995). Witt-Eickshen and Harte (1994) reported relatively high $^{Amph/Cpx}D$ (3 to 8) from peridotite xenoliths of East Eifel, Germany, and ascribed this to lower Na contents of the peridotite system. This is consistent with our results (Table 1). We further propose that $^{Amph/Cpx}D$ are strongly dependent on equilibrium conditions, increasing with a decrease in temperature, because the chemistry, e.g. the Na content, of amphiboles is controlled by temperature in the peridotite system (Evans 1982). This is consistent with the low equilibrium temperature, about 800°C (Wells 1977), for the neoblast assemblage of the Yugu peridotites.

EMPLACEMENT OF YUGU PERIDOTITE

The texture and mineral chemistry have recorded the thermal history of the Yugu peridotites. The primary high-temperature spinel peridotites had started cooling in the upper mantle. Shearing and water supply had been associated with the cooling to produce peridotites with high-temperature anhydrous porphyroclasts and lower-temperature hydrated neoblast assemblages (Fig. 8). The cooling and hydration had been continuous to form tremolitic amphiboles in the matrix, especially on the rim of hornblende neoblasts. This may be equivalent to a successive uplift of the small-scale peridotite bodies along faults from the upper mantle to the surface (Fig. 8). It is noteworthy that plagioclases are totally absent in the Yugu peridotite body: low-Cr# spinels are in intact contact with olivines and pyroxenes in the fertile lherzolites. Plagioclase films are often found around chromian spinel and clinopyroxene porphyroclasts in solid intrusive fertile lherzolites (Komatsu 1974, 1975; Bonatti *et al.* 1986), but not in the Yugu fertile lherzolites. The preservation of the spinel–lherzolite assemblage in the Yugu peridotite body

is possibly ascribed to its small dimension and/or rapid uplift for effective cooling of the mantle slice. Before the rapid uplift, the peridotites should have been cooled and hydrated within the spinel lherzolite stability field because of the change of amphiboles from hornblende to tremolite without production of plagioclase (Fig. 8). The estimated P–T trajectory of the Yugu peridotites (Fig. 8) is similar to that of the Bibong peridotites, but is different from that of the Baekdong peridotites (Fig. 4 of Seo *et al.* 2005). The P–T path of retrogressive metamorphism of metamorphic rocks associated with the peridotites in the Hongseong area (Kim *et al.* 2006) meets the peridotite path under low-P, low-T conditions (Fig. 8).

The age of emplacement of the Yugu peridotites is unfortunately unknown. The preservation of primary mantle minerals in the central part of the body may exclude the possibility that the peridotites had suffered from the regional metamorphism synchronous with the surrounding Precambrian gneiss. It is well known that the solid intrusive mantle peridotites of Precambrian age have been intensely altered. For example, peridotites of the mantle section of Proterozoic ophiolites have been severely altered; their olivines and pyroxenes have been completely altered to serpentines or carbonates (Quick 1990; Gahlan *et al.* 2006). The small bodies of peridotite and serpentinite including the Yugu peridotite body are distributed only near the boundary with the Okcheon Belt (Wee *et al.* 1994). The similarity between the strike of strong foliation of the Yugu peridotites, N30 to 70°E, and the direction of the Jurassic to Cretaceous sinistral fault system (Xu *et al.* 1989; Lee 1999) may be in favor of intrusion of the Yugu peridotites prior to or synchronous with the fault formation. Kim *et al.* (2006) obtained a Triassic age (*ca* 231 Ma) by SHRIMP zircon dating from retrogressed eclogite associated with the Bibong peridotite. Mafic garnet granulites associated with the Baekdong peridotites show Sm–Nd isochron ages of 268–297 Ma (Oh *et al.* 2004). These possibly indicate the emplacement of the Hongseong peridotite bodies in the late Paleozoic to early Mesozoic but before initiation of the sinistral fault system.

Peridotite bodies (Yang *et al.* 1993) are also associated with ultrahigh-pressure metamorphic rocks in the Dabie–Sulu Collision Belt, China, which is considered to be the westward extension of the southwestern part of the Gyeonggi Massif by Oh and co-workers (Oh 2006; Oh *et al.* 2005; Oh & Kusky 2007). The Sulu peridotites, however, exhibit characteristics of higher-pressure equilibration than the Gyeonggi peridotites of Korea. Garnet-bearing lherzolites and harzburgites are predominant in the Sulu Belt (Yang *et al.* 1993; Zhang *et al.* 1994; Yoshida *et al.* 2004). Primary chromian spinels are preserved only in harzburgites with or without garnets (Zhang *et al.* 1994; Yoshida *et al.* 2004). It is noteworthy that the most depleted harzburgite protolith from the Sulu Belt, composed of olivine with $Fo_{91–92}$ and spinel with Cr# = 0.4 to 0.5 (Yoshida *et al.* 2004), is similar to the most depleted harzburgite from the Gyeonggi Massif, Korea (Fig. 4). The compositional range of olivine, Fo_{90} in lherzolites to Fo_{92} in harzburgites (Yang *et al.* 1993; Yoshida *et al.* 2004), is almost the same as that in the spinel lherzolites to harzburgites of the Gyeonggi Massif (Fig. 4). The peridotites from Bibong and Baekdong, which display flat and U-shaped REE patterns (Seo *et al.* 2005), are similar to some Dabie–Sulu garnet peridotites of Type A, which are interpreted to be derived from the mantle wedge (Zhang *et al.* 2000). In summary, the spinel peridotites from the Gyeonggi Massif, South Korea are representative of the upper mantle shallower than the peridotites with or without garnets from the Dabie–Sulu Belt, being in accordance with the difference of P–T paths of associated metamorphic rocks (fig. 5 of Oh *et al.* 2004). The two peridotite suites, however, show similarities in REE distribution pattern and partial melting degree.

As discussed by Arai *et al.* (2001) the arc-type mantle peridotites have been rarely documented as xenoliths from the Asian continental margin. The arc-type peridotites are, however, expected to exist in the upper mantle beneath the continental margin because accretion of arcs to the continental margin is one of the fundamental processes for continent growth (e.g. Taylor & McLennan 1985). As suggested by Arai *et al.* (2001), the sub-arc peridotites or oceanic (ophiolitic) peridotites have been preserved in the continental margin, where accretionry processes are prominent, only when they have been emplaced on or within the crust. Otherwise, they have been possibly replaced or tectonically eroded by continental type peridotites uprisen diapirically (Arai *et al.* 2001).

SUMMARY AND CONCLUSIONS

1. The Yugu peridotite body and some other small bodies show a NNE-trending distribution near the boundary with the Okcheon Belt within the southwestern Gyeonggi Massif, Korea. The

Yugu peridotites are mainly spinel lherzolites with mylonitic to strongly porphyritic textures. Amphiboles, zoned from hornblende in the core to tremolite in the rim, are only found as neoblasts. Dunites, harzburgites and websterites are also found associated with the lherzolites. The exposure of fresh peridotites within small peridotite bodies suggests a relatively young structural zone (fault) penetrating to the spinel lherzolite stability field of the upper mantle.

2. The Fo content of olivines and Cr# of chromian spinels vary from 90 to 91, and from 0.1 to 0.3, respectively, in lherzolites. The harzburgite is more refractory in chemistry, with olivines of Fo_{91} and chromian spinels of Cr# > 0.5. The Na_2O content of clinopyroxenes is relatively low, 0.3 to 0.5wt%, in the most fertile lherzolite. Porphyroclasts have preserved higher temperatures (1000°C of two-pyroxene temperature) than neoblasts (~800°C).
3. Mineral chemistry suggests a resemblance of the Yugu peridotites to sub-arc or abyssal spinel peridotites derived from the upper mantle overlain by relatively thin crust. The harzburgite found both in Yugu and in nearby bodies is equivalent to that most commonly observed in the ophiolitic upper mantle.
4. Pyroxenes and amphiboles exhibit U-shaped REE distribution patterns, indicating involvement of a fluid rich in light REEs and some incompatible trace elements during hydration. The involved fluid may be similar in chemistry to the slab-derived fluids. Hydration or metasomatism was accomplished either within the mantle wedge or after detachment from the mantle within the crust.
5. The spinel peridotites from the Gyeonggi Massif, South Korea are different from the Dabie–Sulu peridotites, some of which contain garnets, and they are in equilibrium at lower pressures than the Dabie–Sulu peridotites. This is consistent with the difference in P–T trajectory between metamorphic rocks from the two belts.

ACKNOWLEDGEMENTS

We thank Mr Y. I. Kim, Mr A. Koyanagi, and Dr K. Matsukage for their collaboration with us in the field. We are grateful to Mr Koyanagi for making thin-sections. Mrs M. Kadoshima helped us to prepare figures. We are grateful to Professor R. Maury, Dr J. Seo, and Professor A. Ishiwatari for constructive comments, and to Professor G. P. Yumul Jr. for editorial management. This study was supported by the Carbon Dioxide Reduction & Sequestration R & D Center (DJ2-201-2-0-0) and by a Grant-in-Aid for Creative Scientific Research (19GS0211).

REFERENCES

ARAI S. 1990. What kind of magmas could be equilibrated with ophiolitic peridotites? *In* Malpas J., Moores E. M., Panayiotou A., & Xenophontos C (eds). *Ophiolites: Oceanic Crustal Analogues. Proceedings of Symposium TROODOS 87*, pp. 557–65, Geological Survey Department and Ministry of Agriculture and Natural Resources, Nicosia.

ARAI S. 1991. Petrological characteristics of the upper mantle peridotites beneath the Japan Island Arcs – Petrogenesis of spinel peridotites. *Soviet Geology and Geophysics (Geologiya i Geofizika)* **32**, 8–26.

ARAI S. 1994. Characterization of spinel peridotites by olivine-spinel compositional relationships: Review and interpretation. *Chemical Geology* **113**, 191–204.

ARAI S., KIDA M., ABE N. & YURIMOTO H. 2001. Petrology of peridotite xenoliths in alkali basalt (11 Ma) from Boun, Korea: An insight into the upper mantle beneath the East Asian continental margin. *Journal of Mineralogical and Petrological Sciences* **96**, 89–99.

AUMENTO F. & LOUBAT H. 1971. The Mid-Atlantic Ridge near 45°N. XVI. Serpentinized ultramafic intrusions. *Canadian Journal of Earth Sciences* **8**, 631–63.

BLUNDY J. D., FALLOON T. J., WOOD B. J. & DALTON J. A. 1995. Sodium partitioning between clinopyroxene and silicate melts. *Journal of Geophysical Research* **100**, 15501–15.

BONATTI E. 1976. Serpentinite protrusions in the oceanic crust. *Earth and Planetary Science Letters* **32**, 107–13.

BONATTI E. 1990. Subcontinental mantle exposed in the Atlantic Ocean on St Peter-Paul islets. *Nature* **345**, 800–2.

BONATTI E., OTTONELLO G. & HAMLYN P. R. 1986. Peridotites from the island of Zabargad (St. John), Red Sea: Petrology and geochemistry. *Journal of Geophysical Research* **91**, 599–631.

CHI J. M. & KIM K. B. 1977. A study on talc mineralization of serpentinite. *Journal of Institute of Mining Geology* **10**, 67–74 (in Korean with English abstract)

COLEMAN R. G. 1977. *Ophiolites*. Springer, New York.

DICK H. J. B. 1989. Abyssal peridotites, very slow spreading ridges and ocean ridge magmatism. *In* Saunders A. D. & Norry M. J. (eds). *Magmatism in the Ocean Basins*. Geological Society Special Publication 42, 71–105. Geological Society of London, London.

DICK H. J. B. & BULLEN T. 1984. Chromian spinel as a petrogenetic indicator in abyssal and alpine-type peridotites and spatially associated lavas. *Contributions to Mineralogy and Petrology* **86**, 54–76.

EVANS B. W. 1977. Metamorphism of alpine peridotite and serpentinite. *Annual Review of Earth and Planetary Sciences* **5**, 397–447.

EVANS B. W. 1982. Amphiboles in metamorphosed ultramafic rocks. *In* Veblen D. R. & Ribbe P. H. (eds). *Amphiboles: Petrology and Experimental Phase Relations. Reviews in Mineralogy, 9B*, pp. 98–113. Mineralogical Society of America, Washington, DC.

GAHLAN H. A., ARAI S., AHMED A. H., ISHIDA Y., ABDEL-AZIZ Y. M. & RAHIM A. 2006. Origin of magnetite veins in serpentinite from the late Proterozoic Bou-Azzer ophiolite, Anti-Atlas, Morocco: An implication for mobility of iron during serpentinization. *Journal of African Earth Sciences* **46**, 318–30.

GASPARIK T. 1987. Orthopyroxene thermometry in simple and complex systems. *Contributions to Mineralogy and Petrology* **96**, 357–70.

GEOLOGICAL AND MINERALOGICAL INSTITUTE OF KOREA. 1973. *Geological Map and Explanatory Text of Seosan-Daejeon Sheet (scale 1:250,000)*. Hallim Publishing Company, Seoul.

GILBERT M. C., HELZ R. T., POPP R. K. & SPEAR F. S. 1982. Experimental studies of amphibole stability. *In* Veblen D. R. & Ribbe P. H. (eds). *Amphiboles: Petrology and Experimental Phase Relations. Reviews in Mineralogy, 9B*, pp. 229–353. Mineralogical Society of America, Washington, DC.

GRÉGOIRE M., MCINNES B. I. A. & O'REILLY S. Y. 2001. Hydrous metasomatism of oceanic sub-arc mantle, Lihir, Papua New Guinea Part 2. Trace element characteristics of slab-derived fluids. *Lithos* **59**, 91–108.

HELLEBRAND E., SNOW J. E., DICK H. J. B. & HOFMANN A. W. 2001. Coupled major and trace elements as indicators of the extent of melting in mid-ocean-ridge peridotites. *Nature* **410**, 677–80.

HWANG J. Y., KIM J. J. & OCK S. S. 1993. Genesis and mineralogy of the serpentinite deposits in the Andong area, Korea. *Journal of Korean Institute of Mining Geology* **26**, 1–10 (in Korean with English abstract).

HWANG J. Y., SHIMODA S., COI S. Y. & KIM J. J. 1988. Aquacreptite from the Ulsan serpentine mine, Korea. *Journal of Mineralogical Society of Korea* **1**, 146–50 (in Korean with English abstract).

IONOV D. A. & HOFMANN A. W. 1995. Nb-Ta-rich mantle amphiboles and micas: Implications for subduction-related metasomatic trace element fractionations. *Earth and Planetary Science Letters* **131**, 341–56.

ISHIDA Y., MORISHITA T., ARAI S. & SHIRASAKA M. 2004. Simultaneous in-situ multi-element analysis of minerals on thin section using LA-ICP-MS. *The Science Reports of Kanazawa University* **48**, 31–42.

ISHIMARU S. & ARAI S. 2008. Calcic amphiboles in peridotite xenoliths from Avacha volcano, Kamchatka, and their implications for metasomatic conditions in the mantle wedge. *In* Coltorti M. & Grégoire M. (eds). *Metasomatism in Oceanic and Continental Lithospheric Mantle*, Geological Society Special Publication 293, 35–55. Geological Society of London, London.

ISHIMARU S., ARAI S., ISHIDA Y., SHIRASAKA M. & OKRUGIN V. M. 2007. Melting and multi-stage metasomatism in the mantle wedge beneath a frontal arc inferred from highly depleted peridotite xenoliths from the Avacha volcano, southern Kamchatka. *Journal of Petrology* **48**, 395–433.

JOHNSON K. T. M., DICK H. J. B. & SHIMIZU N. 1990. Melting inn the oceanic upper mantle: An ion microprobe study of diopsides in abyssal peridotites. *Journal of Geophysical Research* **95**, 2661–78.

KANG P. J. & LIM J. H. 1974. *Geologic Map and Explanatory Text of Gwangjeong Sheet (scale 1:50.000)*. Geological Survey of Korea, Seoul.

KELEMEN P. B., SHIMIZU N. & SALTERS V. J. M. 1995. Extraction of mid-ocean-ridge basalts from the upwelling mantle by focused flow of melt in dunite channels. *Nature* **375**, 747–53.

KIM C.-B., TREK A., CHANG H.-C., PARK Y.-S. & AHN K.-S. 1999. U-Pb zircon ages for Precambrian and Mesozoic plutonic rocks in the Seoul-Cheongju-Chooncheon area, Gyeonggi massif, Korea. *Geochemical Journal* **33**, 379–97.

KIM K. H., PARK J. K., YANG J. M. & SATAKE H. 1993. A study of serpentinization of serpentinite. *Journal of Korean Institute of Mining Geology* **26**, 267–78 (in Korean with English abstract).

KIM S. W., OH C. W., WILLIAMS I. S. *et al.* 2006. Phanerozoic high-pressure eclogite and intermediate-pressure granulite facies metamorphism in the Gyeonggi Massif, South Korea: Implications for the eastward extension of the Dabie-Sulu continental collision zone. *Lithos* **92**, 357–77.

KOMATSU M. 1974. Electron microprobe study of unmixing of aluminous pyroxenes from lherzolite and pyroxenite, Uenzaru, Hidaka mountains, Hokkaido, Japan. *Memoirs of the Geological Society of Japan* **11**, 47–57.

KOMATSU M. 1975. Recrystallization of the high alumina pyroxene peridotite of the Uenzaru area in Hidaka province, Hokkaido, Japan. *Journal of Geological Society of Japan* **81**, 11–28.

KORNPROBST J., OHNENSTETTER D. & OHNENSTETTER M. 1981. Na and Cr contents in clinopyroxenes from peridotites: A possible discriminant between 'sub-continental' and 'sub-oceanic' mantle. *Earth and Planetary Science Letters* **53**, 241–54.

LEAKE B. E., WOOLLEY A. R., ARPS C. E. S. *et al.* 1997. Nomenclature of amphiboles: Report of the subcommittee on amphiboles of the International Mineralogical Association Commission on New Minerals and Mineral Names. *Mineralogical Magazine* **61**, 295–321.

LEE D.-S. 1987. *Geology of Korea*. Kyohak-Sa Publishing Co., Seoul.

LEE D.-W. 1999. Strike-slip fault tectonics and basin formation during the Cretaceous in the Korean Peninsula. *Island Arc* **8**, 218–31.

LEE J. H., GAUDETTE H. E. & HURLEY P. M. 1973. U-Pb zircon age of the Precambrian basement gneisses of South Korea. *In Geology and Ore Deposits 21*, 5–7. Geological and Mineralogical Institute of Korea, Seoul.

LEE S. H. & CHOI G. J. 1994. Geochemistry and chemical equilibria of coexisting minerals in the gneisses around the Daeheung talc deposits, Korea. *Journal of Petrological Society of Korea* **3**, 138–55.

LONGERICH H. P., JACKSON S. E. & GUNTHER D. 1996. Laser ablation inductively coupled plasma mass spectrometric transient signal data acquisition and analyte concentration calculation. *Journal of Analytical Atomic Spectrometry* **11**, 899–904.

MAURY R. C., DEFANT M. J. & JORON J.-C. 1992. Metasomatism of the sub-arc mantle inferred from trace elements in Philippine xenoliths. *Nature* **360**, 661–3.

MELSON W. G., HART S. R. & THOMPSON G. 1972. St. Paul's Rocks, equatorial Atlantic: Petrogenesis, radiometric ages, and implications on sea-floor spreading. *The Geological Society of America Memoir* **132**, 241–72.

MORISHITA T., ISHIDA Y. & ARAI S. 2005a. Simultaneous determination of multiple trace element compositions in thin (<30 μm) layers of BCR-2G by 193 nm ArF excimer laser ablation-ICP-MS: Implications for matrix effect and elemental fractionation on quantitative analysis. *Geochemical Journal* **39**, 327–40.

MORISHITA T., ISHIDA Y., ARAI S. & SHIRASAKA M. 2005b. Determination of multiple trace element compositions in thin (<30 μm) layers of NIST SRM 614 and 616 using laser ablation-inductively coupled plasma-mass spectrometry. *Geostandards and Geoanalytical Research* **29**, 107–22.

OH C. W. 2006. A new concept on tectonic correlation between Korea, china and Japan: Histories from the Late Proterozoic to Cretaceous. *Gondwana Research* **9**, 47–61.

OH C. W. & KUSKY T. 2007. The Late Permian to Triassic Hongseong-Odesan collision belt in South Korea, and its tectonic correlation with China and Japan. *International Geology Review* **49**, 636–57.

OH C. W., CHOI S. G., SONG S. H. & KIM S. W. 2004. Metamorphic evolution of the Baekdong metabasite in the Hongseong area, South Korea and its relationship with the Sulu collision belt of China. *Gondwana Research* **7**, 809–16.

OH C. W., KIM S. W., CHOI S. G., ZHAI M., GUO J. & KRISHNAN S. 2005. First finding of eclogite facies metamorphic event in South Korea and its correlation with the Dabie-Sulu collision belt in China. *Journal of Geology* **113**, 226–32.

OKADA H. & SAKAI T. 1993. Nature and development of Late Mesozoic and Early Cretaceous sedimentary basins in southwest Japan. *Palaeogeography, Palaeoclimatology, Palaeoecology* **105**, 3–16.

OKAMURA H., ARAI S. & KIM Y.-U. 2006. Petrology of fore-arc peridotite from the Hahajima Seamount, the Izu-Bonin arc, with special reference to chemical characteristics of chromian spinel. *Mineralogical Magazine* **70**, 15–26.

PEARCE N. J. G., PERKINS W. T., WESTGATE J. A. *et al.* 1996. A compilation of new and published major and trace element data for NIST SRM 610 and NIST SRM 612 glass reference materials. *Geostandards Newsletter* **21**, 115–44.

QUICK J. E. 1990. Geology and origin of the late Proterozoic Darb Zubaydah ophiolite, Kingdom of Saudi Arabia. *Geological Society of America Bulletin* **102**, 1007–20.

RODEN M. K., HART S. R., FREY F. A. & MELSON W. G. 1984. Sr, Nd and Pb isotopic and REE geochemistry of St. Paul's Rocks: The metamorphic and metasomatic development of an alkali basalt mantle source. *Contributions to Mineralogy and Petrology* **85**, 376–90.

SEO J., CHOI S. G., OH C. W., KIM S. W. & SONG S. H. 2005. Genetic implications of two different ultramafic rocks from Hongseong area in the southwestern Gyeonggi massif, South Korea. *Gondwana Research* **8**, 539–852.

SONG S. H. & SONG Y. S. 2001. Mineralogy and geochemistry of ultramafic rocks from the Singok area, western part of Chungnam. *Economic and Environmental Geology* **34**, 395–415 (in Korean with English abstract).

SONG S. H., CHOI S. G. & WOO J. G. 1997. Genetic implications of ultramafic rocks from the Bibong area in the Kyeonggi gneiss complex. *Economic and Environmental Geology* **30**, 477–91.

SUN S. S. & MCDONOUGH W. F. 1989. Chemical and isotopic systematics of oceanic basalts: Implications for mantle composition and processes. *In* Saunders A. D. & Norry M. J. (eds). *Magmatism in the Ocean Basins*, Geological Society Special Publication 42, 313–45. Geological Society of London, London.

TAYLOR S. R. & MCLENNAN S. M. 1985. *The Continental Crust: Its Composition and Evolution*. Blackwell, Oxford.

UM S. H. & LEE M. S. 1963. *Geologic Map and Explanatory Text of Tae Heung Sheet (scale 1:50.000)*. The Geological Survey of Korea, Seoul.

VANNUCCI R., PICCARDO G. B., RIVALENTI G. *et al.* 1995. Origin of LREE-depleted amphiboles in the subcontinental mantle. *Geochimica et Cosmochimica Acta* **59**, 1763–71.

WEE S.-M., CHOI S.-G. & SO C.-S. 1994. Preliminary study on the ultramafic rocks from the Chungnam Province, Korea. *Economic and Environmental Geology* **27**, 171–80 (in Korean with English abstract).

WELLS P. R. A. 1977. Pyroxene thermometry in simple and complex systems. *Contributions to Mineralogy and Petrology* **62**, 129–39.

WITT-EICKSHEN G. & HARTE B. 1994. Distribution of trace elements between amphibole and clinopyroxene from mantle peridotites of the Eifel (western Germany): An ion-microprobe study. *Chemical Geology* **117**, 235–50.

WOO K. Y., CHOI S. W. & PARK K. H. 1991. Genesis of talc ore deposits in the Yesan area of Chungnam, Korea. *Journal of Korean Institute of Mining Geology* **24**, 363–78.

XU J., TONG W., ZHU G., LIN S. & MA G. 1989. An outline of the pre-Jurassic tectonic framework in east Asia. *Journal of Southeast Asian Earth Science* **3**, 29–45.

YANG J., GODARD G., KIENAST J.-R., LU Y. & SUN J. 1993. Ultrahigh-pressure (60 Kbar) magnesite-bearing garnet peridotites from northeastern Jiangsu, China. *Journal of Geology* **101**, 541–54.

YOSHIDA D., HIRAJIMA T. & ISHIWATARI A. 2004. Pressure-temperature path recorded in the Yangkou garnet peridotite, in Su-Lu ultrahigh-pressure metamorphic belt, eastern China. *Journal of Petrology* **45**, 1125–45.

YUN S. P., MOON H.-S. & SONG Y. 1994. Mineralogy and genesis of the Pyeongan and Daeheung talc deposits in ultramafic rocks, the Yoogoo area. *Economic and Environmental Geology* **27**, 131–45.

ZANETTI A., MAZZUCCHELLI M., RIVALENTI G. & VANNUCCI R. 1999. The Finero phlogopite-peridotite massif: An example of subduction-related metasomatism. *Contributions to Mineralogy and Petrology* **134**, 107–22.

ZHANG R. Y., LIOU J. G. & CONG B. 1994. Petrogenesis of garnet-bearing ultramafic rocks and associated eclogites in the Su-Lu ultrahigh-P metamorphic terrane, eastern China. *Journal of Metamorphic Geology* **12**, 169–86.

ZHANG R. Y., LIOU J. G., YANG J. S. & YUI T.-F. 2000. Petrochemical constraints for dual origin of garnet peridotites from the Dabie-Sulu UHP terrane, eastern-central China. *Journal of Metamorphic Geology* **18**, 149–66.